Abstraction Kinetics of H-Atom by OH Radical from Pinonaldehyde ($C_{10}H_{16}O_2$): Ab Initio and Transition-State Theory Calculations

ARTICLE *in* THE JOURNAL OF PHYSICAL CHEMISTRY A · FEBRUARY 2012

Impact Factor: 2.69 · DOI: 10.1021/jp209208e · Source: PubMed

2 AUTHORS:

Manas Dash
National Chiao Tung University
10 PUBLICATIONS **44** CITATIONS

SEE PROFILE

B. Rajakumar
Indian Institute of Technology Madras
37 PUBLICATIONS **244** CITATIONS

SEE PROFILE

THE JOURNAL OF PHYSICAL CHEMISTRY A

Article

pubs.acs.org/JPCA

Abstraction Kinetics of H-Atom by OH Radical from Pinonaldehyde ($C_{10}H_{16}O_2$): Ab Initio and Transition-State Theory Calculations

Manas Ranjan Dash and B. Rajakumar*

Department of Chemistry, Indian Institute of Technology, Madras, Chennai 600036, India

Supporting Information

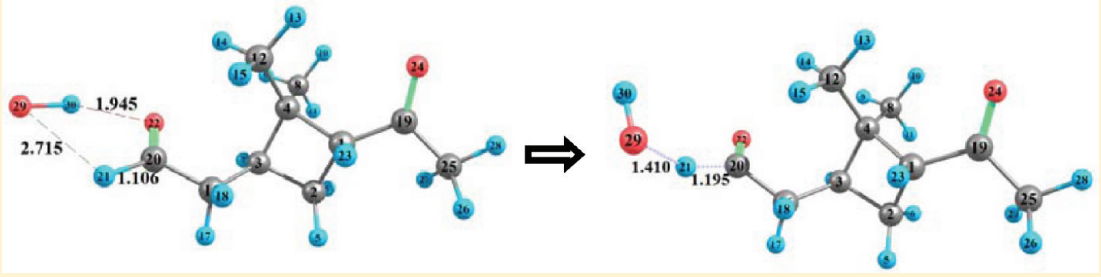

ABSTRACT: The kinetics and abstraction rate coefficients of hydroxyl radical (OH) reaction with pinonaldehyde were computed using G3(MP2) theory and transition-state theory (TST) between 200 and 400 K. Structures of the reactants, reaction complexes (RCs), product complexes (PCs), transition states (TSs), and products were optimized at the MP2(FULL)/6-31G* level of theory. Fifteen transition states were identified for the title reaction and confirmed by intrinsic reaction coordinate (IRC) calculations. The contributions of all the individual hydrogens in the substrate molecule to the total reaction are computed. The quantum mechanical tunneling effect was computed using Wigner's and Eckart's methods (both symmetrical and unsymmetrical methods). The reaction exhibits a negative temperature dependent rate coefficient, $k(T) = (1.97 \pm 0.34) \times 10^{-13} \exp[(1587 \pm 48)/T]$ cm^3 molecule^{-1} s^{-1}, $k(T) = (3.02 \pm 0.56) \times 10^{-13} \exp[(1534 \pm 52/T]$ cm^3 molecule^{-1} s^{-1}, and $k(T) = (4.71 \pm 1.85) \times 10^{-14} \exp[(2042 \pm 110)/T]$ cm^3 molecule^{-1} s^{-1} with Wigner's, Eckart's symmetrical, and Eckart's unsymmetrical tunneling corrections, respectively. Theoretically calculated rate coefficients are found to be in good agreement with the experimentally measured ones and other theoretical results. It is shown that hydrogen abstraction from −CHO position is the major channel, whereas H-abstraction from $-COCH_3$ is negligible. The atmospheric lifetime of pinonaldehyde is computed to be few hours and found to be in excellent agreement with the experimentally estimated ones.

1. INTRODUCTION

Among all the biogenic volatile organic compounds (BVOCs), monoterpenes ($C_{10}H_{16}$) are estimated to be 11% of the total biogenic hydrocarbon emission in the atmosphere.[1] Among all kinds of terpenes emitted in to the troposphere, α-pinene is found to be one of the most abounded one.[1,3] The different types of photo-oxidation products of monoterpenes in the forest atmosphere are reported in the literature.[2−4] Pinonaldehyde ($C_{10}H_{16}O_2$) is the main oxidation product of α-pinene.[1] Pinonaldehyde is produced by the reaction of α-pinene with ozone, as well as OH and NO_3 radicals.[5−7] Pinonaldehyde was detected from pine forest by Yokouchi and Ambe[5] with a concentration of 2.6 ng/m^3 in the atmosphere and 51 ppm (w/w) ratio in aerosol samples. Pinonaldehyde was also detected by Satsumbayashi et al.[8] in rain and snow samples with concentration range between 0.02 and 13 μg/L. Its concentration increases in the night time and decreases in the day time due to its further decomposition by photochemical reactions in the atmosphere.[8] Hallquist et al.[13] estimated the lifetime of pinonaldehyde to be few hours with respect to photodissociation, reaction with OH and NO_3 radicals. The detailed degradation mechanism of pinonaldehyde by reaction with OH radicals described by Fantechi et al.[9] and Grosjean et al.[6] leads to the formation of smaller fragments of carbonyl compounds like CH_3CO, CH_2O, CH_2CHO, etc. These compounds further decompose to the formation of PANs (peroxyacyl nitrates), CO, and glyoxal.

Several kinetic experimental investigations were reported on the reaction of pinonaldehyde with OH radicals. Nozière et al.,[10] Alvarado et al.,[11] Glasius et al.,[12] and Hallquist et al.[13] have carried out the reactions using relative-rate methods with different detection techniques such as FTIR spectroscopy, GC, and HPLC to obtain the rate coefficients. These reported room temperature rate coefficients fall in the range of $(4-9) \times 10^{-11}$ cm^3 molecule^{-1} s^{-1}. Recently, Davis et al.[14] have measured the temperature dependent (between 297 and 374 K) rate coefficient for this reaction to be $k(T) = (4.5 \pm 1.3) \times 10^{-12} \exp[(600 \pm 100)/T]$ cm^3 molecule^{-1} s^{-1}. In their investigations, they have used the pulsed laser photolysis technique

Special Issue: A. R. Ravishankara Festschrift

Received: September 23, 2011
Revised: February 21, 2012
Published: February 22, 2012

   dx.doi.org/10.1021/jp209208e | J. Phys. Chem. A 2012, 116, 5856−5866

with laser induced fluorescence (PLP-LIF) detection of OH radicals. Kwok and Atkinson[16] estimated the rate coefficient to be $k(298K) = 2.4 \times 10^{-11}$ cm^3 molecule^{-1} s^{-1} using structure activity relationships (SAR), with 85% contribution of aldehydic-H abstraction. The "adjusted" SAR approach by Vereecken and Peeters[15] predicted the rate coefficient for this reaction to be $k(298K) = 3.5 \times 10^{-11}$ cm^3 molecule^{-1} s^{-1} with a branching ratio of 59:23:14 for abstraction of the aldehydic-H, exocyclic-CH_2-hydrogen, and tertiary-H abstraction, respectively. They studied the C−H bond strengths in pinonaldehyde theoretically using B3LYP-DFT/6-31G(d,p) and correlated with H-abstraction reaction rates.

Although several experimental and theoretical investigations are reported on the title reaction, a detailed study on the contribution of each hydrogen toward the global rate coefficient in the temperature range 200−400 K (relevant to the Earth's atmosphere) is lacking.

In this paper, we present the H-abstraction rate coefficient for the reaction of pinonaldehyde with OH radical in the temperature range 200−400 K. The rate coefficients are computed using conventional transition-state theory (CTST) in combination with G3(MP2) theory. The contribution of each hydrogen in pinonaldehyde toward the global rate coefficient in the given temperature range is reported in this paper.

We present geometries, energies, and vibrational frequencies of each stationary point, i.e., reactants, reactant complexes (RCs), transition states (TSs), product complexes (PCs), and products. We also report the atmospheric lifetime of this compound, due to its reaction with OH radical. The oxidation of pinonaldehyde by OH radicals is initiated by H-atom abstraction at different C-sites (labeling of the different carbons follows that of ref 15) are given by the following scheme.

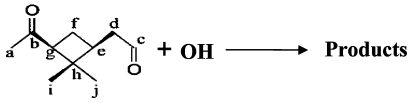

2. COMPUTATIONAL METHODS

The geometries of the reactants (pinonaldehyde ($C_{10}H_{16}O_2$), OH), four RCs (RC1, RC4, RC5, RC11), fifteen TSs (TS1 to TS15), four PCs (PC1, PC4, PC5, PC11), and products of all abstraction channels were optimized with the second-order Møller−Plesset[17] MP2(FULL) level of theory including all electrons in correlation with the Pople basis set 6-31G*, which are internally available with the Gaussian program suite.[18] All TSs that correspond to the abstraction of hydrogen by the OH radical from different carbon sites of pinonaldehyde are summarized in Table 1. All the reactants, RCs, PCs, and products were identified with zero imaginary frequency (number of imaginary (NIMG) = 0), and each transition state was identified with one imaginary frequency (NIMG = 1). The structures and normal modes were viewed in Gaussview,[19] and the normal mode corresponding to the reaction coordinate was observed to be consistent with the reaction of interest. Structural parameters obtained at MP2(FULL)[17] level of theory and Gaussian-3[20] methods, namely, G3(MP2)[21] were used for all energetic and kinetic calculations.

Table 1. Transition States Correspond to the Abstraction of Hydrogen by OH Radical from Different Carbon Sites of Pinonaldehyde

H-abstraction site	TSs
C_c	TS1
C_d	TS2 and TS3
C_e	TS4
C_g	TS5
$C_{i/j}$	TS6, TS7, TS8 TS9, TS10, and TS11
C_f	TS12 and TS13
C_a	TS14 and TS15

3. RATE COEFFICIENTS

Rate coefficients for hydrogen abstraction reaction from the substrate, pinonaldehyde, were computed using conventional transition-state theory (CTST).[22]

$$k(T) = l\frac{k_B T}{h}\left(\frac{Q_{\ddagger}}{Q_R}\right)\exp\left(\frac{-\Delta E_0^{\ddagger}}{RT}\right)$$

where l is the reaction path degeneracy, ‡ represents the transition state, k_B is the Boltzmann constant, and h is Planck's constant. T is the temperature in Kelvin, $Q_{\ddagger}$ and Q_R are the partition functions for the TS and reactants in the GS. $\Delta E_0^{\ddagger}$ is the molar zero-point energy inclusive barrier height, and R is the universal gas constant. The electronic partition function of the OH radical was evaluated by taking the splitting of 139.7 cm^{-1} in the $^2\Pi$ GS, into account.[23] Quantum mechanical tunneling effect along the reaction coordinates are included by temperature dependent transmission coefficient $\Gamma(T)$. The final rate coefficients were calculated using the equation

$$k_{\Gamma}(T) = \Gamma(T)\, k(T)$$

The values of $\Gamma(T)$ were calculated by using three methods, namely Wigner's method[24] and symmetrical and unsymmetrical Eckart's methods.[25−27] The conventional transition-state theory coupled with Wigner's and Eckart's tunneling methods was used previously by various other research groups[28−31] and by our group[32−36] to compute the rate coefficients for hydrogen abstraction reactions at lower temperatures. The agreement between the computed rate coefficients of various molecules reported[28−36] with OH radicals, using the above said methods were found to be reasonably in good agreement with the experimentally measured ones. TST calculations were performed using two models, namely harmonic oscillator (HO) and hindered rotor (HR) model. The method proposed by Truhlar and his co-workers[37] was used in our calculations, for HR model. The three or four lowest-frequency modes corresponding to hindered rotation of the reactant and all the TSs were treated as hindered rotors.

4. RESULTS AND DISCUSSION

4.1. Electronic Structures and Energetics. Figure 1 shows the calculated molecular geometries of reactants, RCs, TSs, PCs, and products at the MP2(FULL)/6-31G* level of theory. All the structural parameters of reactants, RCs, TSs, PCs, and products are given in the Supporting Information (Table S-I). Vibrational analyses were carried out for all the reactants, RCs, TSs, PCs, and products at the same level of theory and are given in the Supporting Information (Table S-II). It has been checked that there is no significant spin

dx.doi.org/10.1021/jp209208e | J. Phys. Chem. A 2012, 116, 5856−5866

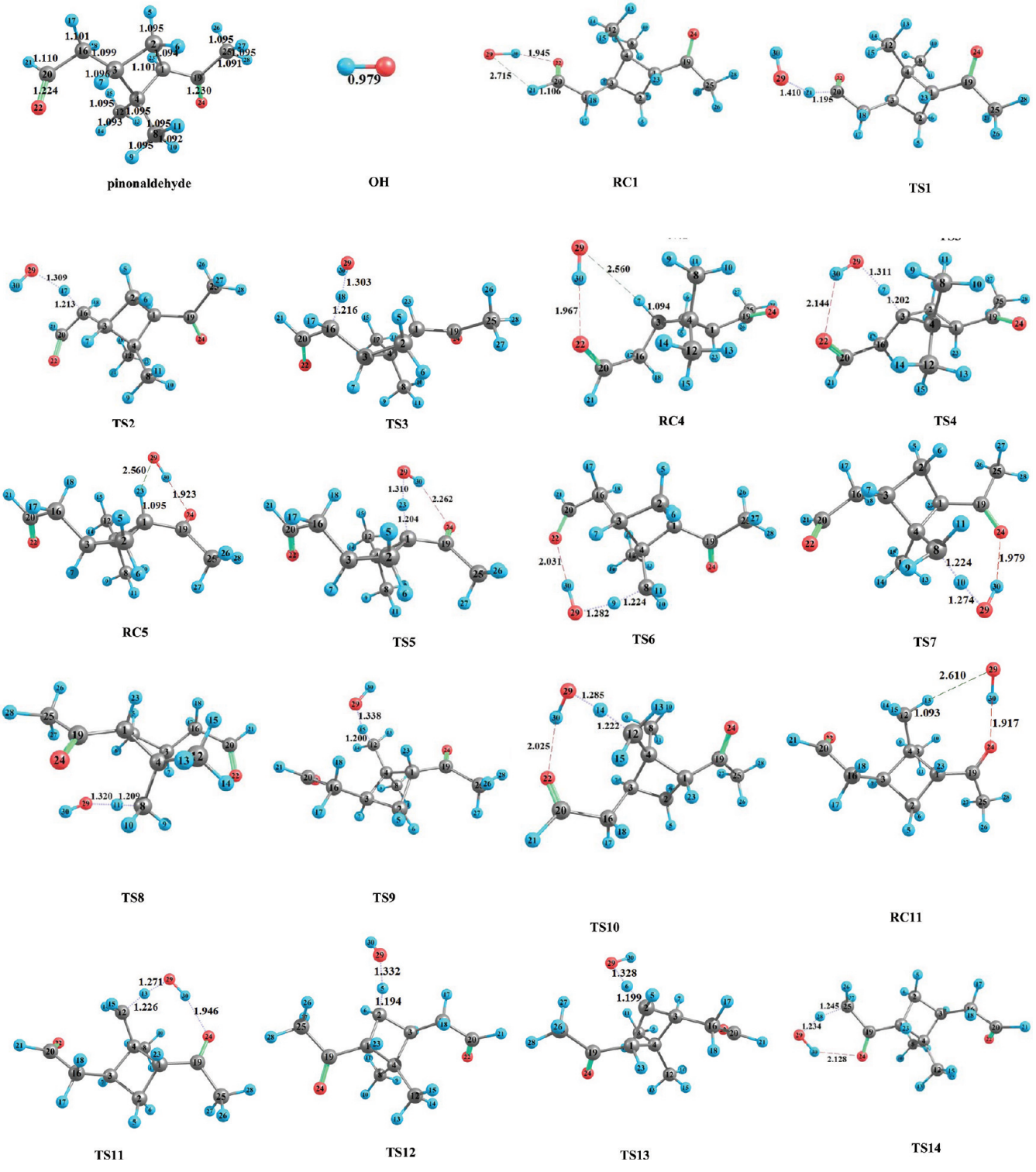

Figure 1. continued

dx.doi.org/10.1021/jp209208e | *J. Phys. Chem. A* 2012, 116, 5856−5866

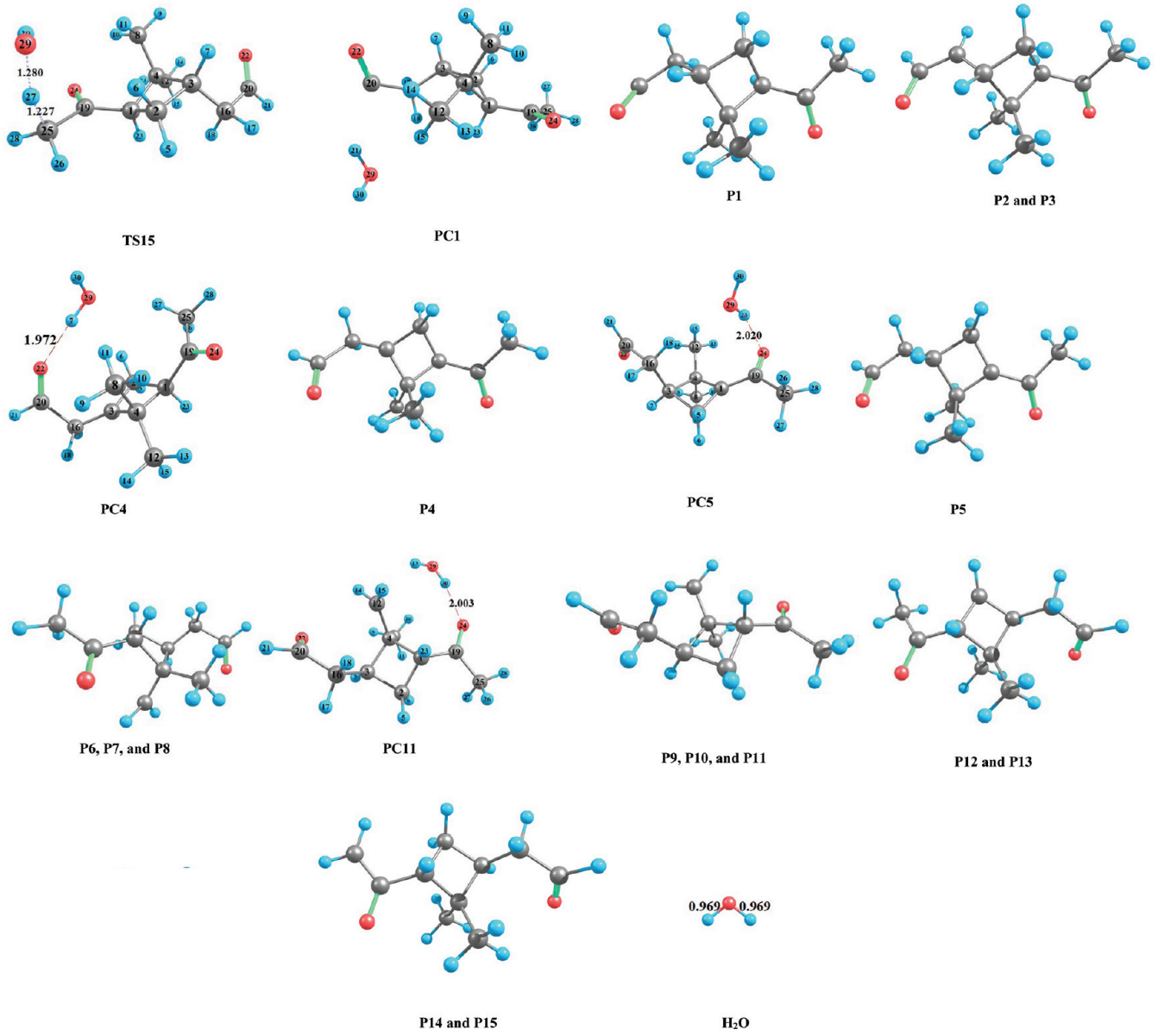

Figure 1. Geometries of the reactants, reaction complexes, transition states, product complexes, and products optimized at the MP2(FULL)/6-31G* level of the theory. Blue represents hydrogen, black represents carbon, and red represents oxygen atoms in the structures. The bond lengths (Å) given on the structures are obtained at MP2(FULL)/6-31G* theory.

contamination ($\langle S^{**}2\rangle \sim 0.75$) for all TSs. The spin contamination ($\langle S^{**}2\rangle$) values of all TSs optimized at MP2(FULL)/6-31G* level of theory are given in the Supporting Information (Table S-III). The TSs appeared to be more similar to reactant geometries than product geometries. During the formation of the transition states, the most important parameters that have to be considered are the C−H bond length of the leaving hydrogen and the newly formed bond between the leaving hydrogen and oxygen atom in the OH radical. The elongations of breaking C−H bond lengths are varied between 7% and 12% in all the TSs, as compared to normal C−H bond lengths in pinonaldehyde. However, in the case of a newly formed bond, i.e., H−O bond, the bond lengths are varied between 22% and 31% when compared with the H−O bond length in a water molecule optimized at the same level of theory. In all TSs the elongation of the breaking bond (C−H) is less than that of the forming bond, suggesting that all the TSs are reactant-like, that the reaction proceeds through "early transition state". The variation of the bond length between the C−H and O−H bonds between TSs and reactants are given in Supporting Information (Table S-IV). Intrinsic reaction coordinate (IRC) calculations were carried out to confirm that all the transition states follow distinctly different reaction paths and also to see that the transition states are connected to the reactants and products. The energy profiles for all the TSs obtained with IRC calculations at the MP2(FULL)/6-31G* level of theory, except TS4, which is optimized at the B3LYP/6-31G* level of theory are given in Figure S-I (Supporting Information). The reaction pathway of TS4 could not be obtained at MP2(FULL)/6-31G*. However, the same was obtained at B3LYP/6-31G*. Energy level diagrams for the title reaction through all fifteen TSs are given in Figure 2. The entropy of activation ($\Delta S^{\ddagger}$) and barrier heights ($\Delta E_0^{\ddagger}$) for the reaction are computed and listed in Table 2. The calculated

dx.doi.org/10.1021/jp209208e | J. Phys. Chem. A 2012, 116, 5856−5866

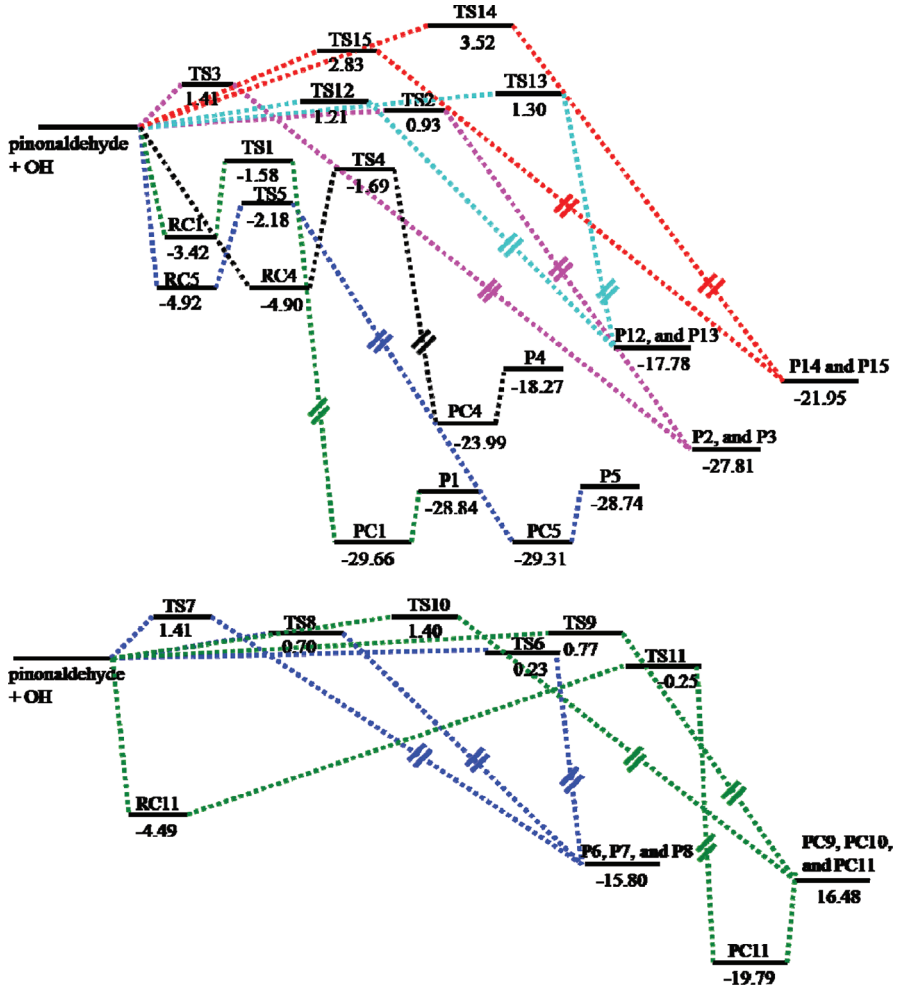

Figure 2. Energy level diagram for the reaction through all the fifteen transition states obtained at the G3(MP2) level of theory. The energies are given in the units of kcal mol^{-1}.

Table 2. Barrier Heights [$\Delta E_0^{\ddagger}$, kcal mol^{-1}], Entropy of Activation [$\Delta S^{\ddagger}$(298K), cal mol^{-1} K^{-1}] Obtained at the G3(MP2) Level of Theory

TSs	$\Delta E_0^{\ddagger}$	$\Delta S^{\ddagger}$(298K)
TS1	−1.580	−28.115
TS2	0.932	−26.574
TS3	1.407	−30.158
TS4	−1.688	−31.252
TS5	−2.181	−33.802
TS6	0.227	−33.176
TS7	1.411	−32.990
TS8	0.714	−34.275
TS9	0.773	−30.580
TS10	1.400	−32.151
TS11	−0.252	−33.151
TS12	1.211	−27.058
TS13	1.299	−30.996
TS14	3.516	−30.935
TS15	2.828	−33.135

barrier heights with the G3(MP2) method would have a possible error bar of 1−2 kcal mol^{-1}; therefore, the calculated thermal reaction rates may change accordingly. Out of fifteen TSs, four TSs (TS1, TS4, TS5, and TS11) have lower energy than the reactant's energies. In the case of negative energy channels, i.e., when the barrier is below the separated reactant level, the reactants always form a weakly bound reactant complexes (RCs) before proceeding to TSs, and then break up to form a weakly bound product complexes (PCs) before proceeding to the products.

$$\text{reactants} \rightarrow \text{RCs} \rightarrow \text{TSs} \rightarrow \text{PCs} \rightarrow \text{products}$$

The existence and importance of reactant complexes in the reaction of OH radicals with carbonyl compounds were reported earlier.[31,42,43] The kinetic parameters computed using this methodology are observed to be in excellent agreement with experimentally measured ones. Aloisio and Francisco[42] discussed the structure and energetics of the reactant complexes involving the hydroxyl radical with formaldehyde, acetaldehyde, and acetone using density functional theory. The same approach is used in our present investigation using the ab initio method. The energy differences between the reaction complexes (RC1, RC4, RC5, and RC11) and the reactants are 3.42, 4.90, 4.92, and 4.49 kcal mol^{-1}, respectively. The energy differences between product complexes (PC1, PC4, PC5, and PC11) and products are 2.4, 7.41, 2.76, and 3.56 kcal mol^{-1}, respectively. The complete information of energetics of reactants, RCs, TSs, PCs, and products (in hartree) are given in the Supporting Information (Table S-V).

dx.doi.org/10.1021/jp209208e | J. Phys. Chem. A 2012, 116, 5856−5866

The formation of the pre reactive complex is expected to suppress the methyl group rotation and distinguishing the two hydrogens from the third one. In the present test molecule there are three methyl groups and they have shown different behaviors from one another. Surprisingly, in the case of the CH_3 group attached to the carbonyl group and in the case of the second methyl group (C_8), no pre-reaction complexes were formed during the reaction. In the case of the third methyl group (C_{12}), one pre-reaction complex was formed (before TS11 is formed) and could not suppress the free rotation of the methyl group.

Two types of attractive interactions were observed in the RCs. One of these interactions is observed to be very strong between the hydrogen atom of OH radical and one of the oxygen atoms of pinonaldehyde. The other interaction is formed between the oxygen atom in OH and one of the hydrogens of the nearest carbon atoms. One of the structural differences among the RCs is the presence or absence of hydrogen bonding between the hydrogen atom in OH and the oxygen atom in pinonaldehyde. In RC1 and RC4 the hydrogen bond is formed between the H-atom of the OH radical and the O-atom of the −CHO group, forming five-membered and seven-membered ringlike structures, respectively. In RC5 and RC11 the hydrogen bond is formed between the H-atom of the OH radical and the O-atom of the $-COCH_3$ group, forming six-membered and seven-membered ringlike structures, respectively. The stabilizing hydrogen bond lengths are found to be 1.95 Å (RC1), 1.96 Å (RC4), and 1.92 Å (both RC5 and RC11). The reactant complexes formed between the OH radical and the $-COCH_3$ group are found to be stronger than reactant complexes formed between the OH radical and the −CHO group of pinonaldehyde. This is also true for the reactant complexes formed between the OH radical with acetaldehyde and acetone.[42] Alvarez-Idaboy et al.[43] have theoretically studied the importance of reactant complexes in the abstraction reactions of hydrogen from aldehydes by OH radicals.

Out of the identified fifteen TSs, seven TSs (TS4, TS5, TS6, TS7, TS10, TS11, and TS14) are found to be influenced by strong hydrogen bonding, and the rest of the eight TSs (TS1, TS2, TS3, TS8, TS9, TS12, TS13, and TS15) have no influence of hydrogen bonding. It is important to see how hydrogen bonding influences energetics as well as kinetics of the reaction. Both TS4 and TS5 correspond to tertiary hydrogen abstraction on C_e and C_g carbons. In TS4 the hydrogen bond is formed between the H-atom of the OH radical and the O-atom of the −CHO group, whereas in the case of TS5 hydrogen bonding is observed with the O-atom of the $-COCH_3$ group. The hydrogen bond in TS4 is shorter (2.14 Å) than the corresponding hydrogen bond in TS5 (2.26 Å). Therefore, TS4 is expected to have a lower energy barrier than TS5. But the energy barriers observed are quite opposite. Table 2 shows that TS4 (−1.6 kcal mol^{-1}) has a 0.5 kcal mol^{-1} higher barrier than TS5 (−2.1 kcal mol^{-1}). This contrast behavior in the energy barrier may be due to the formation of different types of ringlike structures through hydrogen bonding. During the process of abstraction of hydrogen, a six-membered ring through hydrogen bonding is formed in TS5, which is more stable than TS4 because a seven-membered ring is formed through hydrogen bonding in the case of TS4. Also, the O-atom of the $-COCH_3$ group is more electronegative than the O-atom of the −CHO group. So, the interaction with the H-atom of the OH group is more stabilized in TS5 than TS4. Also, TS5 is more stable than TS4 because channel 5 is exothermic by 10 kcal mol^{-1} compared to channel 4. Similarly, TS6, TS7, TS10, and TS11 belong to H-abstraction from the same type of primary CH_3 groups on C_i and C_j carbons. The stabilized hydrogen bond interaction is found to be strongest for TS11 (1.94 Å), followed by TS7 (1.97 Å), TS10 (2.02 Å), and TS6 (2.03 Å). Table 2 shows that the following increasing order of energy barriers: TS11 (−0.25 kcal mol^{-1}) < TS6 (0.23 kcal mol^{-1}) < TS10 (1.40 kcal mol^{-1}) ≈ TS7 (1.41 kcal mol^{-1}). TS11 is found to be most stabilized among these TSs due to its shortest hydrogen bond. TS14 also has a similar type of stabilized six-membered hydrogen bond (2.12 Å) with a barrier energy of 3.5 kcal mol^{-1}. TS15 is lower in energy than TS14 even though the latter has a strong hydrogen bond. The most possible reason for this anomalous behavior could be that, in the case of TS14, all six atoms forming the six-membered ring via hydrogen bonding are lying almost in a plane, where the strain could be higher. However, in the case of TS15, all six atoms do not exist in a single plane, in which case the strain is lower and hence TS15 is more stabilized. Therefore, TS15 is lower in energy than TS14 by about 1.3 kcal mol^{-1}. From Table 2, it is clear that in most of the cases the entropy of activation ($\Delta S^{\ddagger}$) of the non-hydrogen-bonded TSs are higher than those of hydrogen-bonded TSs. The hydrogen-bonded transition states are more stabilized than the non-hydrogen-bonded ones because the hydrogen-bonded transition states are less disordered than the non-hydrogen-bonded ones. The standard enthalpy (ΔH^0), free energy (ΔG^0), and entropy change (ΔS^0) of the reaction through all the H-abstraction reaction channels are given in Table 3. Reaction through the aldehydic H-abstraction channel on the C_c carbon is found to be more exothermic than ketonic H-abstraction channels on the C_a carbon. Among two tertiary H-abstraction sites (C_e and C_g), abstraction from the C_g carbon is found to be more exothermic than that from the C_e carbon. Nearly similar exothermicities are observed for the abstraction of hydrogen from the C_i, C_j, and C_f carbons.

Table 3. Heat of Reaction [ΔH^0(298K), kcal mol^{-1}], Gibbs Free Energy [ΔG^0(298K), kcal mol^{-1}], and Entropy of Reaction [ΔS^0(298K), cal mol^{-1} K^{-1}] Obtained at the G3(MP2) Level of Theory

H-abstraction site	ΔH^0(298K)	ΔG^0(298K)	ΔS^0(298K)
C_c	−28.546	−29.719	3.938
C_d	−27.549	−29.030	4.968
C_e	−17.729	−19.927	7.377
C_g	−28.246	−30.008	5.911
C_i	−15.373	−16.711	4.490
C_j	−16.021	−17.486	4.917
C_f	−17.343	−19.160	6.099
C_a	−21.903	−22.306	1.358

4.2. Reaction Path Analysis. Intrinsic reaction coordinate calculations (IRC) were performed at the MP2(FULL)/6-31G* level of theory to obtain the minimum energy path (MEP) and also to ensure that all the transition states identified follows distinctly different reaction paths. Figure 3 shows the classical potential energy (V_{MEP}), the vibrational ground-state adiabatic potential energy (V_a^G), and the zero-point energy (ZPE) for the aldehydic H-abstraction reaction (TS1) as a function of the intrinsic reaction coordinate at the MP2-(FULL)/6-31G* level of theory, where $V_a^G = V_{MEP}$ + ZPE.

dx.doi.org/10.1021/jp209208e | J. Phys. Chem. A 2012, 116, 5856−5866

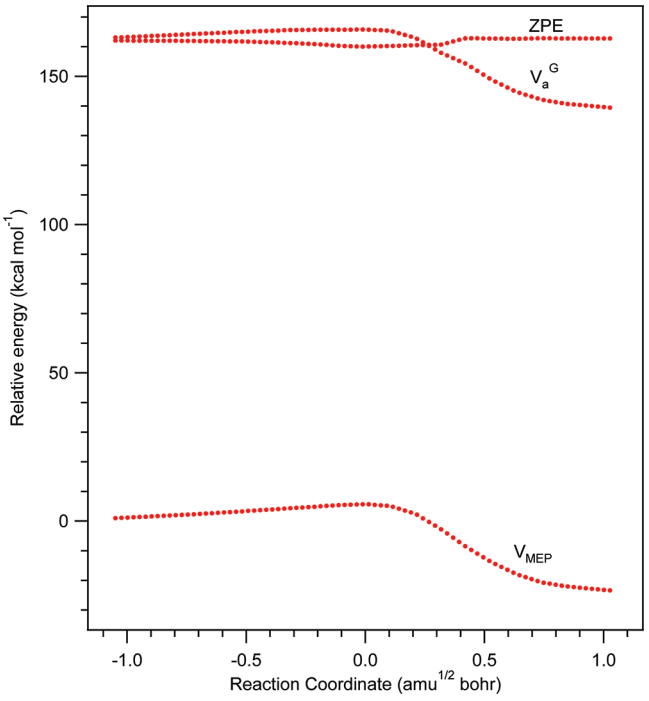

Figure 3. Classical potential energy curve (V_{MEP}), vibrational ground-state adiabatic potential energy (V_a^G), and zero-point energy (ZPE) curve as functions of reaction coordinate at the MP2(FULL)/6-31G* level for TS1.

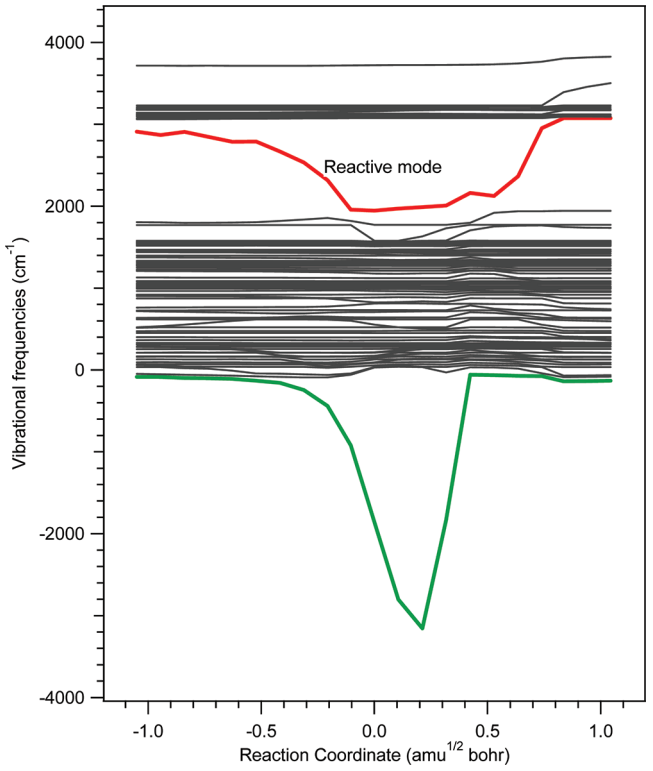

Figure 4. Generalized normal-mode vibrational frequencies as a function of reaction coordinate at the MP2(FULL)/6-31G* level for TS1.

Because of the similarity, the corresponding plots for TS4 and TS5 are depicted in Figure S-II (Supporting Information). As seen from Figure 3, there is a shallow flat minimum on the ZPE curve so that the location of the maxima of the classical and the vibrationally adiabatic ground-state energy curves essentially coincide, indicating the variational effect to be almost negligible. The variational effects for hydrogen abstraction reaction are well documented and illustrated in the literature.[38−40]

Figure 4 shows the variation of the generalized normal-mode vibrational frequencies along the MEP for TS1. In this abstraction reaction, 84 vibrational frequencies exist along the MEP. Most of them do not change significantly when going from the reactants to products, except the vibrational modes indicated by red and green lines. The red line indicates the "reactive mode" and has a dramatic drop near the saddle point, which corresponds to a C−H stretching mode close to the reaction center. This kind of mode is known to be typical character of hydrogen transfer reaction.[44] The green line indicates the imaginary vibrational frequencies for TS1 along the reaction path, with a sudden drop near the saddle point region. The variation of the generalized normal-mode vibrational frequencies along the MEP for TS4 and TS5 are given in Figure S-III (Supporting Information).

4.3. Kinetic Analysis. There are several experimentally measured and theoretically computed rate coefficients available in the literature for the title reaction.[10−16] However, no temperature dependent studies based on theoretical methods are reported so far. In the present investigation, the calculations were carried out in the temperature range 200−400 K with an interval of 25 K. The optimized parameters and harmonic frequencies used in CTST calculations were obtained at the MP2(FULL)/6-31G* level of theory. The thermal rate coefficients were computed by taking the barrier energies for all TSs, through the direct mechanism (R → TS → P). In the case of positive barrier channels, the forward barrier from R to TS was used for Eckart's symmetrical tunneling corrections and both the forward barrier and backward barrier from P to TS were used for Eckart's unsymmetrical tunneling corrections. The imaginary frequencies associated with the transition states were used for Wigner's tunneling corrections. Four out of fifteen transition states, namely TS1, TS4, TS5, and TS11, were observed to have negative energy barriers. No doubt they do contribute significantly to the total rate coefficient when compared with the positive energy barrier transition states (cf. Table 5). However, if we have a careful look at the energy parameters (cf. Figure 2), it is very obvious that the negative energy barriers are not too much higher when compared with the other eleven positive energy transition states (cf. Figure 2). Before computing the rate coefficients, we have carried out the variational analysis for this reaction to check if any variational effect is there and found the variational effect to be almost negligible. Therefore, we did not do any CVTST (canonical variational transition-state theory) calculations and carried out only CTST calculations. Recently, several research groups[38,40,47] have followed the same kind of approach for H-abstraction reactions of various molecules. In their studies, they have not observed any difference between the computed rate coefficients following both CVTST and CTST methods.

In our calculations, the thermal rate coefficients are computed by taking the negative barrier energies for submerged TSs, through the direct mechanism (R → TS → P). But the tunneling corrections have been calculated for those TSs through the complex mechanism (R → RC → TS → PC → P). The submerged transition states were treated differently than the nonsubmerged transition states, as the contribution to the

dx.doi.org/10.1021/jp209208e | J. Phys. Chem. A 2012, 116, 5856−5866

Table 4. Arrhenius Parameters for the Title Reaction of Pinonaldehyde + OH at the G3(MP2) Level of Theory

	Wigner		Eckart symmetrical		Eckart unsymmetrical		experiment[14]	
model	A ($\times 10^{-13}$)[a]	E_a/R[b]	A ($\times 10^{-13}$)[a]	E_a/R[b]	A ($\times 10^{-13}$)[a]	E_a/R[b]	A ($\times 10^{-13}$)[a]	E_a/R[b]
HO[c]	1.26 ± 0.18	−1121 ± 41	1.88 ± 0.3	−1086 ± 44	0.26 ± 0.09	−1698 ± 105	45 ± 13	−600 ± 100
HR[c]	1.98 ± 0.34	−1587 ± 48	3.0 ± 0.56	−1534 ± 52	0.47 ± 0.19	−2041 ± 110		

[a]Units: cm^3 $molecule^{-1}$ s^{-1}. [b]Units: K. [c]The quoted uncertainties are the 2σ (95% confidence limits) precision from the linear least-squares fit of the kinetic parameters obtained for the reaction through each transition state.

total rate coefficient is a maximum in the case of the former ones. In these submerged TSs, reaction complexes (RCs) and product complexes play a very important role in tunneling. The forward barrier height from RC to TS (known as effective barrier,[46] $E_{eff} = E_{TS} - E_{RC}$) was used for Eckart's symmetrical tunneling corrections. Both the forward barrier from RC to TS and the backward barrier from PC to TS were used for Eckart's unsymmetrical tunneling corrections. At high pressures one can assume that these complexes are in equilibrium with the reactants, and then the rate coefficient expression proves to be the same as if there was no complex at all, but only if one does not include any tunneling correction. However, when the magnitude of tunneling is calculated using Eckart's model potential, it does matter what the barrier height is: is it measured from the bottom of the well or from the energy level of the noninteracting reactants? In our calculations the barrier heights are measured from the bottom of the well of RCs. The same methodology for tunneling corrections was used by Alvarez-Idaboy et al.[43] and Galano et al.[46] Alvarez-Idaboy et al.[48] have used CTST to calculate the rate coefficients for the addition reactions of substituted ethenes with OH radicals, which are going through submerged TSs. They also have followed a similar kind of mechanism (R → RC → TS → P), which is similar to the current proposed mechanism (R → RC → TS → PC → P). The overall rate coefficients for these substituted ethenes + OH addition reactions agreed very well with the experimental results. The tunneling coefficients obtained by using all methods are given in Table S-VI (Supporting Information).

When one looks at the energetics of TS1 (−1.58 kcal mol^{-1}), TS4 (−1.68 kcal mol^{-1}), TS5 (−2.18 kcal mol^{-1}), and TS11 (−0.25 kcal mol^{-1}), it is very clear that TS11 is less stabilized and TS5 is more stabilized. Therefore, the contribution from TS5 is expected to be more when compared with the other three transition states. However, the contribution of TS1 is greater than the rest of the three transition states. This anomaly can be explained, if the effective barriers ($E_{eff} = E_{TS} - E_{RC}$) of these transition states are considered. The E_{eff} for TS1 (1.84 kcal mol^{-1}) is the least when compared to those of other three transition states, i.e., TS4 (3.22 kcal mol^{-1}), TS5 (2.74 kcal mol^{-1}), and T11 (4.24 kcal mol^{-1}). TS1 corresponds to the aldehydic hydrogen, and as expected, the contribution is more and this abstraction pathway is the more favorable one in the OH initiated oxidation of pinonaldehyde.

The global rate coefficient is obtained by summing all the computed rate coefficients between all the transition states.

Two models, namely, harmonic oscillator (HO) and hindered rotor (HR),[37] have been used to compute the rate coefficients. The torsional motion was treated as either HO or HR for the calculation of pre-exponential factors. The reduced moments of inertia for each frequency which were treated as hindered internal rotors and the corresponding torsional barriers are given in Table S-VII (Supporting Information). The rate coefficients obtained using HO model are certainly poorer than those with the HR model when compared with the experimentally measured rate coefficients. Table 4 shows the Arrhenius parameters obtained for the reaction of OH radical with pinonaldehyde at the G3(MP2) level of theory, using HO and HR models. It is clear from Table 4 that the pre-exponential factors obtained using the HO model are lower than those obtained with the HR model. The computed pre-exponential factors are 1 order of magnitude lower than the experimentally measured ones. The experimentally measured E_a's are smaller than the theoretically computed ones. Figure 5

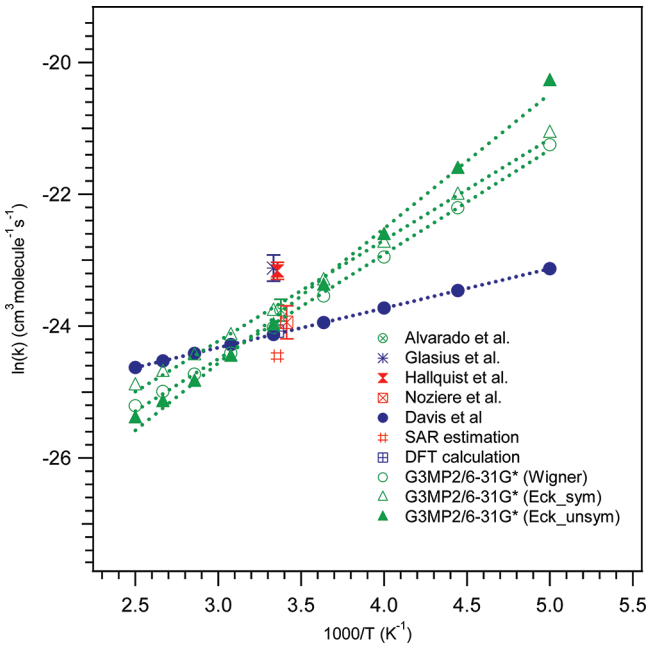

Figure 5. Arrhenius plot for the rate coefficient data obtained for the OH radical reaction with pinonaldehyde over the temperature range 200−400 K. The data are identified by different symbols defined in the figure.

depicts the Arrhenius plot of the rate coefficient data obtained using Wigner's method and symmetrical and unsymmetrical Eckart's tunneling methods with the G3(MP2) theory using the HR model. The calculated rate coefficients using the Arrhenius expression $k(T) = (4.5 \pm 1.3) \times 10^{-12} \exp[(600 \pm 100)/T]$ cm^3 $molecule^{-1}$ s^{-1} reported by Davis et al.[14] in the complete temperature range (200−400 K) are also included in Figure 5. Although the rate coefficients obtained using all three types of tunneling methods were found to be in reasonably good agreement with the literature values particularly at room temperatures, the rate coefficients obtained using Wigner's and Eckart's unsymmetrical functional are very close to the experimentally reported ones.[14] The computed rate coefficients show slight deviation at either extremes of the studied temperature range. This deviation may be because the rate

dx.doi.org/10.1021/jp209208e | J. Phys. Chem. A 2012, 116, 5856−5866

Table 5. Rate Coefficients (Units: cm^3 molecule^{-1} s^{-1}) of H-Abstraction from C-Sites in Pinonaldehyde and Corresponding Percentage at 300 K Using G3(MP2) Theory

H-abstraction site	k_{site} Wigner	K_{site} Eckart symmetrical	k_{site} Eckart unsymmetrical	k_{site} DFT calculation[15]
C_c (%)	2.23×10^{-11} (60.5)	2.8×10^{-11} (59.1)	2.1×10^{-11} (55.5)	2.1×10^{-11} (59)
C_d (%)	3.61×10^{-12} (9.8)	5.36×10^{-12} (11.4)	1.62×10^{-12} (4.3)	8.0×10^{-12} (23)
C_e (%)	2.41×10^{-12} (6.5)	3.08×10^{-12} (6.5)	5.07×10^{-12} (13.4)	3.0×10^{-12} (8.5)
C_g (%)	4.86×10^{-12} (13)	5.69×10^{-12} (12)	7.75×10^{-12} (20)	2.0×10^{-12} (5.7)
$C_{i/j}$ (%)	1.53×10^{-12} (4.1)	2.27×10^{-12} (4.8)	1.00×10^{-12} (2.7)	0.8×10^{-12} (2.3)
C_f (%)	2.15×10^{-12} (5.8)	2.92×10^{-12} (6.2)	1.37×10^{-12} (3.6)	0.5×10^{-12} (1)
global	3.7×10^{-11} (~100)	4.7×10^{-11} (~100)	3.8×10^{-11} (~100)	3.5×10^{-11} (~100)

coefficient is the combination of the pre-exponential factor and the activation energy at a given temperature.

The theoretically computed rate coefficients in the present investigation and experimentally determined[14] rate coefficients have shown negative temperature dependence over the temperature range of this study. The calculated rate coefficients at 300 K using the HR model with G3(MP2) theory using Wigner's method and symmetrical and unsymmetrical Eckart's tunneling corrections are 3.69×10^{-11}, 4.72×10^{-11}, and 3.78×10^{-11} cm^3 molecule^{-1} s^{-1}, respectively. Here it is clear that these values are very close to one another, irrespective of the method used for tunneling corrections. The computed rate coefficients at 300 K are in good agreement with the experimentally measured rate coefficients, $(3.46 \pm 0.4) \times 10^{-11}$ cm^3 molecule^{-1} s^{-1} at 297 K by Davis et al.,[14] $(4.8. \pm 0.8) \times 10^{-11}$ cm^3 molecule^{-1} s^{-1} at 296 K by Alvarado et al.,[11] and $(4.0 \pm 1.0) \times 10^{-11}$ cm^3 molecule^{-1} s^{-1} at 293 K by Noziere et al.[10] However, the experimentally measured rate coefficients, $(9.1 \pm 1.8) \times 10^{-11}$ cm^3 molecule^{-1} s^{-1} at 300 K by Glausius et al.[12] and $(8.72 \pm 1.14) \times 10^{-11}$ cm^3 molecule^{-1} s^{-1} at 298 K by Hallquist et al.,[13] are approximately 2 times larger than our numbers. Interestingly, our rate coefficients are very close to the predicted one using SAR methods, 2.4×10^{-11} cm^3 molecule^{-1} s^{-1} at 298 K by Kwok and Atkinson.[16] The "adjusted" SAR approach of Veereecken and Peeters[15] predicted the rate coefficient for H-abstraction from pinonaldehyde with the OH radical at 298 K to be 3.5×10^{-11} cm^3 molecule^{-1} s^{-1}, which is also in excellent agreement with the rate coefficients calculated in the present study. At lower temperatures the calculated rate coefficients are higher than the experimental ones, because the calculated activation energies are more negative (−3 to −4 kcal mol^{-1}). Veereecken and Peeters[15] estimated a branching ratio of 59:23:14 for aldehydic-H (from C_c), exocyclic-CH_2-H (from C_d), and tertiary-H (from C_g and C_e) abstraction. In our calculations the corresponding ratios are found to be 61:10:20 using Wigner's tunneling corrections, 59:11:19 using symmetrical Eckart's tunneling corrections, and 56:4:33 using unsymmetrical Eckart's tunneling corrections. The contributions of all the H-abstractions from C-sites in pinonaldehyde at 300 K to the global rate coefficient using G3(MP2) theory with the HR model are given in Table 5 along with the estimated values at 298 K by Veereecken and Peeters.[15] The contribution of H-abstraction from the $-COCH_3$ group (C_a) to the global rate coefficients seems to be completely negligible. From Table 5, it is concluded that H-abstraction from aldehydic carbon (C_c) and one of the tertiary carbons (C_e) is observed to be the most favorable reaction sites for the title reaction. Veereecken and Peeters[15] predicted that the abstraction of tertiary hydrogen from a carbon in a four-membered ring would not to be influenced by ring strain. The contribution of H-abstraction from tertiary carbons (C_g and C_e) to the global rate coefficients were found to be more than H-abstraction from exocyclic CH_2-hydrogens (from C_d) in our calculations, and it may be due to the stability of the tertiary radical formed during the abstraction. Figure 6 shows the branching ratios for temperature dependent rate coefficients for all the reaction channels of the title reaction. It is clear from the plot that the branching ratios computed using Wigner's and symmetrical Eckart's tunneling corrections are almost identical. Also, the contribution of H-abstraction channels from the C_c, C_g, C_e, C_d, $C_{i/j}$, and C_f carbons to the total rate coefficients was found to be 50−62%, 7−25%, 4−6%, 2−19%, 1−6%, and 0.7−4% using Wigner's method and symmetrical Eckart's tunneling corrections, and 37−54%, 11−45%, 4−6%, 0.4−10%, 2−9%, and

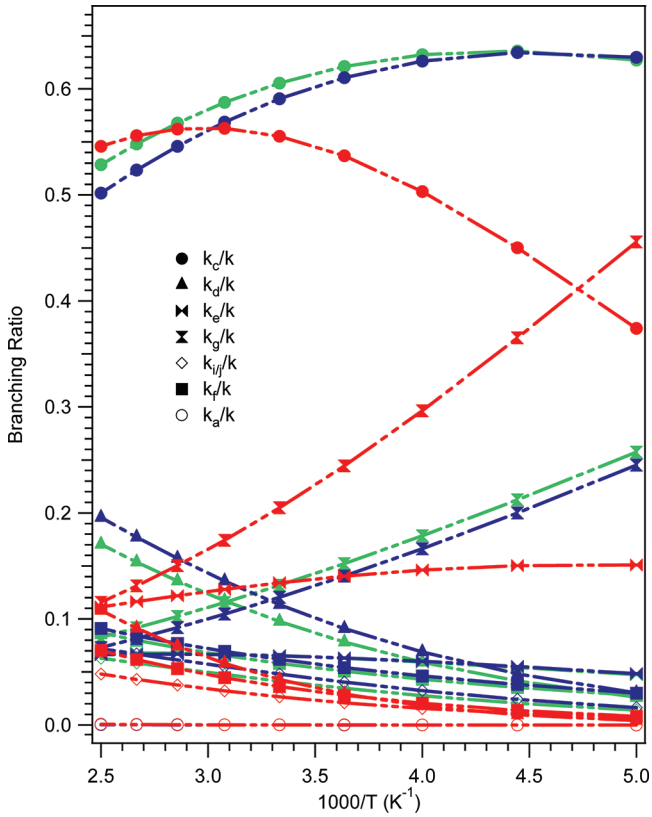

Figure 6. Calculated branching ratios vs 1000/T in the temperature range 200−400 K for the reaction of pinononaldehyde + OH. The green line corresponds to Wigner's tunneling correction, the blue line corresponds to symmetrical Eckart's tunneling correction, and the red line corresponds to unsymmetrical Eckart's tunneling correction. The data are identified by different symbols and are defined in the above figure.

dx.doi.org/10.1021/jp209208e | J. Phys. Chem. A 2012, 116, 5856−5866

0.8−7% using unsymmetrical Eckart's tunneling corrections, respectively, in this studied temperature range. The contribution of H-abstraction from C_a carbon could be neglected in this temperature range.

4.4. Atmospheric Lifetimes. Pinonaldehyde is lost in the atmosphere due to photolysis and reaction with OH, Cl, NO_3, and O_3. The concentration of [OH] was taken as 1.0×10^6 molecules cm^{-3}, as reported by Prinn et al.[41] as the global average concentration to derive OH driven atmospheric lifetimes of pinonaldehyde. The calculated lifetimes of pinonaldehyde estimated by the G3(MP2) level of theory with Wigner's method and symmetrical Eckart's and unsymmetrical Eckart's methods are 2.85 2.28, and 2.33 h, respectively. These values are in very good agreement with the experimentally reported atmospheric lifetime of pinonaldehyde with respect to the reaction with OH, by Hallquist et al.[13] (3.2 h) and Alvarado et al.[11] (2.9 h) and Calogirou et al.[45] (2 h). In general, the atmospheric lifetime of any compound that is released into the atmosphere depends on the rates at which it is lost via various physical and chemical processes. Usually, the atmospheric lifetimes of most compounds varies from several years to a few seconds, because of all the possible processes. In the case of pinonaldehyde, the atmospheric lifetime due to its reactivity with OH radicals is a few hours, which is very short. Therefore, pinonaldehyde is lost in the atmosphere within a few hours after it is released.

5. CONCLUSION

In this paper, the hydrogen abstraction reaction of pinonaldehyde with OH radical was investigated using high-level ab initio methods. All possible reaction pathways are explored. The importance of reaction complexes and product complexes are described in this manuscript. The dominant reaction channel is the abstraction of hydrogen from the aldehydic site. The OH driven atmospheric lifetime of pinonaldehyde because of its reactivity with OH radical is computed to be about 2.5 h, which is very short. Much more reliable rate coefficients can be obtained, if the experiments are carried out with deuterated aldehydic site and such experiments are planned in our research group.

■ ASSOCIATED CONTENT

Supporting Information

Tables S-I to S-VIII (Cartesian coordinates, vibrational frequencies, spin contamination values, bond distances, energies, Wigner's method and Eckart's tunneling correction, moments of inertia, rate coefficients) and Figures S-I to S-III (energy level diagram, energy curves, vibrational frequences vs reaction coordinate). This material is available free of charge via the Internet at http://pubs.acs.org.

■ AUTHOR INFORMATION

Corresponding Author

*E-mail: rajakumar@iitm .ac.in.

Notes

The authors declare no competing financial interest.

■ ACKNOWLEDGMENTS

All calculations reported in this paper are carried out at the High Performance Computing Environment Facility, Computer Centre of Indian Institute of Technology Madras (IITM). We thank the center and especially Mr. Ravichandaran for valuable support. We thank Dr. Mohamad Akbar Ali for useful discussions.

■ REFERENCES

(1) Guenther, A.; Hewitt, C. N.; Erickson, D.; Fall, R.; Geron, C.; Graedel, T.; Harley, P.; Klinger, L.; Lerdau, M.; McKay, W. A.; et al. *J. Geophys. Res.* **1995**, *100*, 8873−8892.
(2) Kavouras, I. G.; Mihalopoulos, N.; Stephanou, E. G. *Nature* **1998**, *395*, 683−686.
(3) Kavouras, I. G.; Mihalopoulos, N.; Stephanou, E. G. *Geophys. Res. Lett.* **1999**, *26*, 55−58.
(4) Calogirou, A.; Larsen, B. R.; Kotzias, D. *Atmos. Environ.* **1999**, *29*, 1423−1439.
(5) Yokouchi, Y.; Ambe, Y. *Atmos. Environ.* **1985**, *19*, 1271−1276.
(6) Grosjean, D.; Williams, E. L. II; Seinfeld, J. H. *Environ. Sci. Technol.* **1992**, *26*, 1526−1533.
(7) Wangberg, I.; Barnes, I.; Becker, K. H. *Environ. Sci. Technol.* **1997**, *31*, 2130−2135.
(8) Satsumbayashi, H.; Nishizawa, H.; Yokouchi, Y.; Ueada, H. *Chemosphere* **2001**, *45*, 887−891.
(9) Fantechi, G.; Vereecken, L.; Peeters, J. *Phys. Chem. Chem. Phys.* **2002**, *4*, 5795−5805.
(10) Nozière, B.; Spittler, M.; Ruppert, L.; Barnes, I.; Becker, K. H.; Pons, M.; Wirtz, K. *Int. J. Chem. Kinet.* **1999**, *31*, 291−301.
(11) Alvarado, A.; Arey, J.; Atkinson, R. *J. Atmos. Chem.* **1998**, *31*, 281−297.
(12) Glasius, M.; Calogirou, A.; Jensen, N. R.; Hjorth, J.; Nielsen, C. J. *Int. J. Chem. Kinet.* **1997**, *29*, 527−533.
(13) Hallquist, M.; Wängberg, I.; Ljungström. *Environ. Sci. Technol.* **1997**, *31*, 3166−3172.
(14) Davis, M. E.; Talukdar, R. K.; Notte, G.; Ellison, G. B.; Burkholder, J. B. *Environ. Sci. Technol.* **2007**, *11*, 3959−3965.
(15) Vereecken, L.; Peeters, J. *Phys. Chem. Chem. Phys.* **2002**, *4*, 467−472.
(16) Kwok, E. S. C.; Atkinson, R. *Atmos. Environ.* **1995**, *29*, 1685−1695.
(17) Moller, C.; Plesset, M. S. *Phys. Rev.* **1934**, *46*, 618−622.
(18) Frisch, M. J.; Trucks, G. W.; Schlegel, H. B.; Scuseria, G. E.; Robb, M. A.; Cheeseman, J. R.; Montgomery, J. A., Jr.; Vreven, T.; Kudin, K. N.; Burant, J. C.;et al. *Gaussian 03*, Revision C. 02; Gaussian, Inc.: Wallingford, CT, 2004.
(19) Dennington, I. I. R.; Keith, T.; Millam, J.; Eppinnett, K.; Hovell, W. L.; Gilliland, R. *GaussView*, Version 3.09; Semichem, Inc.: Shawnee Mission, KS, 2003.
(20) Curtiss, L. A.; Redfern, P. C.; Raghavachari, K.; Rassolov, V.; Pople, J. A. *J. Chem. Phys.* **1998**, *109*, 7764−7776.
(21) Curtiss, L. A.; Redfern, P. C.; Raghavachari, K.; Rassolov, V.; Pople, J. A. *J. Chem. Phys.* **1999**, *110*, 4703−4709.
(22) Wright, M. R. *Fundamental Chemical Kinetics and Exploratory Introduction to the Concepts*; Ellis Horwood: Chichester, U.K., 1999.
(23) Ogura, T.; Miyoshi, A.; Koshi, M. *Phys. Chem. Chem. Phys.* **2007**, *9*, 5133−5142.
(24) Wigner, E. P. Z. *Phys. Chem. B* **1932**, *19*, 203−216.
(25) Eckart, C. *Phys. Rev.* **1930**, *35*, 1303−1309.
(26) Johnston, H. S.; Heicklen, J. J. *Phys. Chem.* **1962**, *66*, 532−533.
(27) Louis, F.; Gonzalez, C. A.; Huie, R. E.; Kurylo, M. J. *J. Phys. Chem. A* **2000**, *104*, 8773−8778.
(28) Chandra, A. K.; Uchimaru, T. J. *Phys. Chem. A* **2000**, *104*, 8535−8539.
(29) Korchowiec, J.; Kawahara, S.-I.; Matsumura, K.; Uchimara, T.; Surgie, M. *J. Phys. Chem. A* **1999**, *103*, 3548−3553.
(30) Zhang, M.; Lin, Z.; Song, C. *J. Chem. Phys.* **2007**, *126*, 34307.
(31) Alvarez-Idaboy, J. R.; Cruz-Torres, A.; Galano, A.; Ruiz-Santoyo, M. E. *J. Phys. Chem. A* **2004**, *108*, 2740−2749.
(32) Ali, M. A.; Rajakumar, B. *J. Comput. Chem.* **2010**, *31*, 500−509.
(33) Ali, M. A.; Rajakumar, B. *J. Mol. Struct: THEOCHEM.* **2010**, *949*, 73−81.
(34) Kaliginedi, V.; Ali, M. A.; Rajakumar, B. *Int. J. Quantum Chem.* **2012**, *112*, 1066−1077.

(35) Ali, M. A.; Rajakumar, B. *Int. J. Chem. Kinet.* **2011**, *43*, 418−430.
(36) Ali, M. A.; Upendra, B.; Rajakumar, B. *Chem. Phys. Lett.* **2011**, *511*, 440−446.
(37) Chuang, Y.; Truhlar, D. G. *J. Chem. Phys.* **2000**, *112*, 1221−1228.
(38) Wang, Y.; Liu, J-y.; Li, Z-s.; Wang, L.; Wu, J-y.; Sun, C-c. *J. Phys. Chem. A* **2006**, *110*, 5853−5859.
(39) Sun, H.; Law, C. K. *J. Phys. Chem. A* **2010**, *114*, 12088−12098.
(40) Gao, H.; Liu, J-y.; Sun, C-c. *J. Chem. Phys.* **2009**, *130*, 224301.
(41) Prinn, R.; Weiss, R.; Millar, B.; Jaung, J.; Alyea, F.; Cunnold, D.; Fraser, P.; Hartley, D.; Simmonds, P. *Science* **1995**, *269*, 187−192.
(42) Aloisio, S.; Francisco, J. S. *J. Phys. Chem. A* **2000**, *104*, 3211−3224.
(43) Alvarez-Idaboy, J. R.; Mora-Diez, N.; Boyd, R. J.; Vivier-Bunge, A. *J. Am. Chem. Soc.* **2001**, *123*, 2018−2024.
(44) Kraka, E.; Dunning, T. H., Jr. In *Advances in Molecular Electronic Structure Theory*; Dunning, T. H., Jr., Ed.; JAI Press: Greenwich, 1990, Vol. *1*, p 938.
(45) Calogirou, A.; Jensen, N. R.; Nielsen, C. J.; Kotzias, D.; Hjorth, J. *Environ. Sci. Technol.* **1999**, *33*, 453−460.
(46) Galano, A.; Alvarez-Idaboy, J. R.; Ruiz-Santoyo, M. E.; Vivier-Bunge, A. *J. Phys. Chem. A* **2005**, *109*, 169−180.
(47) Yang, L.; Liu, J-y.; Li, Z-s. *J. Phys. Chem. A* **2008**, *112*, 6364−6372.
(48) Alvarez-Idaboy, J. R.; Mora-Diez, N.; Vivier-Bunge, A. *J. Am. Chem. Soc.* **2000**, *122*, 3715−3720.